Periodic orbits of nonscaling Hamiltonian systems from quantum mechanics

Cite as: Chaos **5**, 261 (1995); https://doi.org/10.1063/1.166075
Submitted: 29 November 1993 • Accepted: 08 August 1994 • Published Online: 14 August 1998

M. Baranger, M. R. Haggerty, B. Lauritzen, et al.

Periodic orbits of nonscaling Hamiltonian systems from quantum mechanics

M. Baranger, M. R. Haggerty,[a] and B. Lauritzen[b]
Center for Theoretical Physics, Laboratory for Nuclear Science, and Department of Physics, Massachusetts Institute of Technology, Cambridge, Massachusetts 02139

D. C. Meredith
Department of Physics, University of New Hampshire, Durham, New Hampshire 03824

D. Provost[c]
Chemical Physics Theory Group, Department of Chemistry, University of Toronto, Toronto M5S 1A1, Canada

(Received 29 November 1993; accepted for publication 8 August 1994)

Quantal (E,τ) plots are constructed from the eigenvalues of the quantum system. We demonstrate that these representations display the periodic orbits of the classical system, including bifurcations and the transition from stable to unstable. © *1995 American Institute of Physics.*

I. INTRODUCTION

In the past 30 years we have learned a great deal about classical mechanics. We have gone from a world view in which integrable systems were dominant to one in which systems displaying soft chaos (i.e., a mixture of chaos and regularity) are considered generic. This shift has caused us to bring the relationship between classical and quantum mechanics under fresh scrutiny because the methods that worked for integrable systems are inapplicable to chaotic ones.

Semiclassical mechanics provides the bridge between classical and quantum descriptions of nature. In the semiclassical description of quantum mechanics, classical trajectories play a central role as they correspond to stationary phases of Feynman's path-integral. The work of Gutzwiller[1] and Balian and Bloch[2] show how to obtain the eigenvalue spectrum from the periodic orbits and their properties (period, action, stability, Maslov index). For integrable systems this is equivalent to the better known torus-quantization of the early days of semiclassical quantization.[3] For chaotic systems however, the periodic orbit expansion (in its different forms) constitutes the only semiclassical quantization scheme known. Unfortunately this approach is difficult in practice since infinite, nonconvergent sums are involved. In recent years, a great deal of effort has gone into improving the convergence and practicality of these methods, with some success.[4]

While learning about quantum mechanics from classical mechanics has practical problems, the approach in the other direction does not. It is not hampered by infinite sums, since there is no exponential proliferation of eigenvalues analogous to that of long periodic orbits. For example, Balian and Bloch[2] found the periodic orbits of the spherical billiards in its Fourier transformed spectra. A similar analysis was done by Wintgen,[5] who Fourier transformed the spectrum of the hydrogen atom in a uniform magnetic field, and found peaks at the scaled actions of the periodic orbits. Holle *et al.* and Du and Delos[6] looked at the Fourier transforms of the experimental absorption spectra of the same system and, again, saw closed orbits. Argaman *et al.*[7] calculated a classical quantity (correlations of classical actions) by assuming spectral density correlations given by Random Matrix Theory and found agreement for the hyperbola billiards, the cat map, the baker's map, and the zeros of the Riemann zeta function.

We shall propose a method to generate a quantal version of the classical plots of period τ vs energy E for nonscaling systems using the quantum eigenvalues alone. Similar work has been done by Malta *et al.*;[8] however their (E,τ) plots also required knowledge of the eigenvectors. To see that such a project might work, consider the evolution of a quantum wave packet. If the wave packet is launched along a classical periodic orbit, and if the period is short enough, the orbit stable enough, and $\hbar$ small enough, the packet will return to its initial position (more or less intact) after a time τ, the period of the orbit. Hence the information about classical periodic orbits must be in the quantum mechanics. We will derive a formula to extract that information from the quantum eigenvalues.

Why is it interesting to extract classical behavior from quantum mechanics? First, one can adopt the fundamental point of view that microscopic systems are quantum mechanical in nature and semiclassical approximations may provide a simple understanding of otherwise complex behavior. Second, it allows for verification of the classical–quantal correspondence even in systems where enumeration of periodic orbits is difficult, and periodic orbit sums are almost unusable. Finally, there are systems for which the quantum mechanics is actually easier, and with this approach one can obtain valuable information about their classical limit; this includes systems that have been studied only experimentally.

In the present study we will focus on nonscaling systems displaying soft chaos. Scaling systems are those that have the same dynamics at all energies (e.g., billiards) except for trivial changes in scale; they have received most of the at-

[a]Present address: Kellogg Radiation Laboratory, California Institute of Technology, Pasadena, California 91125.
[b]Present address: Niels Bohr Institute, Copenhagen, Denmark.
[c]Present address: Department of Physics and Astronomy, Laurentian University, Sudbury P3E 2C6, Canada.

 1054-1500/95/5(1)/261/10/$6.00

tention so far. They are easier to analyze, and in many cases they display hard chaos. But, quite often, the methods used to analyze them do not work for the more generic nonscaling systems with soft chaos. However, we shall confine ourselves in the applications to two coordinate space dimensions; this is not a generic thing to do, but it is a place to start.

This paper is organized as follows: in Sec. II we review classical (E,τ) plots and in Sec. III we motivate and derive the corresponding quantal (E,τ) plot. In Sec. IV we discuss the semiclassical limit of the quantal plot and in particular the validity of the diagonal approximation, which simplifies the connection to the classical periodic orbits. Finally, in Sec. V we present numerical results for the quantal (E,τ) plots and verify that these are peaked at the classical periodic orbits.

II. CLASSICAL (E,τ) PLOT

Periodic orbits are central to our understanding of classical dynamics of chaotic systems and also in making the transition to quantum mechanics. In the chaotic component of a classical Hamiltonian system the typical (i.e., nonperiodic) trajectories wander ergodically over a significant fraction of phase space. These trajectories are incomprehensible and unknowable since they display no regular pattern and have an infinite time scale. Periodic orbits, on the other hand, can be thoroughly explored. They are presumably dense in phase space and at finite time scales may mimic typical dynamics arbitrary well, the longer orbits doing a better job than the short ones. Moreover, the families of periodic orbits have the unique and wonderful property that they continue smoothly across the fractal boundary between the regular region and the chaotic region of phase space, thus being the only unifying agents between these two disparate regions. And yet, it is easy to tell which region the periodic orbit is in, since it is stable in the regular region and unstable in the chaotic one. Truly, the periodic orbits are in many ways the key to the classical dynamics or, in Poincaré's words, "they are, so to speak, the only breach through which we might try to penetrate into a stronghold hitherto reputed unassailable".[9]

A global view of the periodic orbit structure of a system is obtained by looking for the relation between the energy E and the period τ of the orbits. It is natural and customary to present the results as a two-dimensional plot of E vs τ because the classical periodic orbits form one-parameter families, and along such a family E and τ vary smoothly.[10] Such a plot is characteristic of the system under study and it contains much useful information, for both the regular and the chaotic regions, including stability and instability, period n-tuplings, bifurcations, etc. The (E,τ) plot for a scaling system is simpler because it is independent of energy and therefore displays no bifurcations. But for a nonscaling system, it makes a perfect complement to a good set of Poincaré sections. Numerical methods for finding all periodic orbits and following families of periodic orbits are given in Refs. 11–13.

As an example of these (E,τ) plots, we examine the periodic orbits of the Nelson Hamiltonian

$$H(p_x,p_y,x,y)=\frac{p_x^2}{2}+\frac{p_y^2}{2}+0.05x^2+\left(y-\frac{x^2}{2}\right)^2. \tag{1}$$

For details of the classical calculations, a general survey of the periodic families, and a classification of bifurcations, see Refs. 10–12. Figure 1 of the present paper shows three classical (E,τ) plots taken from Ref. 10. Figure 1(a) gives an overall picture of the main symmetric (in x) families. It is very incomplete; many other known families are not shown on it. Figure 1(b) shows the families associated with the low-energy horizontal oscillations. Figure 1(c) gives details of what happens for short periods and a fairly large range of energies. In the figures, families of stable orbits are shown by thick lines, while unstable orbits are given by thin lines. Period n-tuplings are indicated by horizontal lines; isochronous branchings occur whenever a single line splits into two lines.

In the next section we will derive equivalent quantum (E,τ) plots. These plots will be fuzzy approximations to the classical plots, showing ridges along the families of periodic orbits. Only in the semiclassical limit will the quantal plots reduce to the classical plots with delta-type singularities along the periodic orbits.

III. QUANTAL (E,τ) PLOT

The classical periodic orbits are buried in the quantum mechanics in many ways, hence there are several ways to motivate and derive the quantal (E,τ) plot. As the quantal plots are constrained only in their semiclassical forms, where they should mimic classical (E,τ) plots, we may adopt different definitions of the quantum plot.

We begin with one simple derivation, by noting that in the quantal problem the effect of the periodic orbits, stable or unstable, is to introduce correlations in the energy spectrum. For chaotic systems, we do not have an explicit quantization scheme, but in the semiclassical limit we can express the spectral density $\rho(E)=\mathrm{Tr}\,\delta(E-\hat{H})$ as a series of oscillating terms (in E) with characteristic frequencies given by the classical periodic orbits [cf. Eq. (14) below]. The Fourier transform of $\rho(E)$ should thus be strongly peaked at the periods of the periodic orbits, and in particular at the periods of the shortest periodic orbits.

While this is indeed correct for scaling systems where the dynamics is independent of the energy, for generic nonscaling systems the periods, and therefore the frequencies, are not constant. Following a suggestion by Saraceno,[14] for nonscaling systems we limit the Fourier transform to a classically small energy interval around E so that the frequency does not vary significantly over this interval. If we limit the integration in energy with a Gaussian, this is known as a Gabor transform.[15] This method will become more accurate as $\hbar\to 0$ and there are more eigenvalues in each classically small energy interval ΔE around E. Therefore we define the quantal (E,τ) plot as follows:

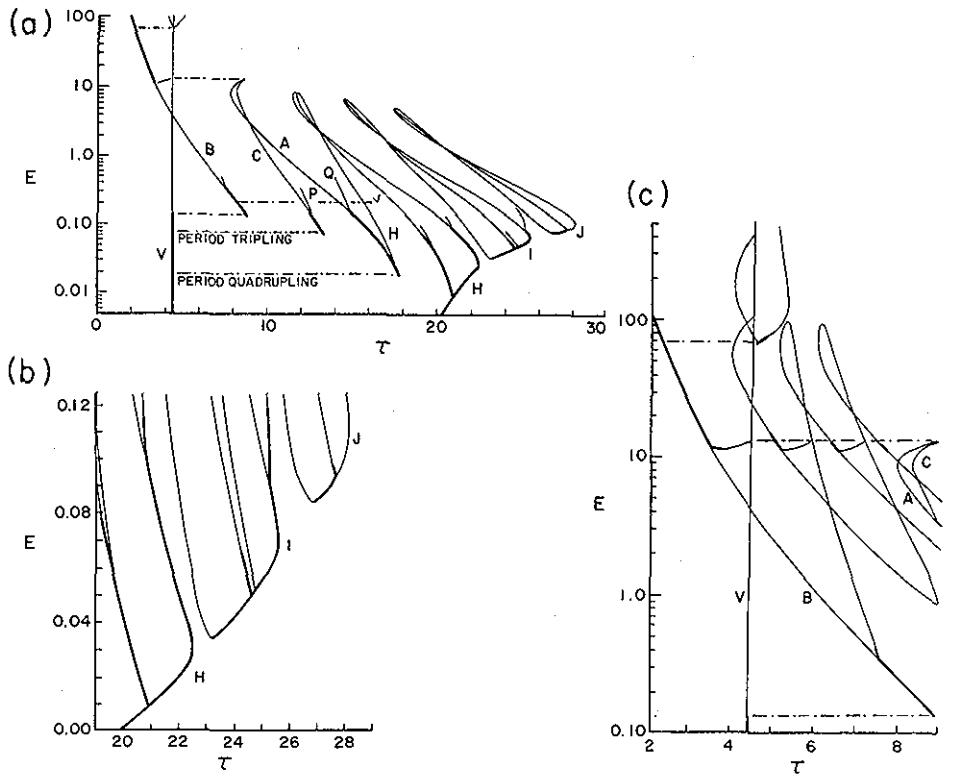

FIG. 1. Examples of classical (E,τ) plots of the Nelson potential, taken from Ref. 10. The full lines indicate a stable orbit, the light an unstable. A line which ends abruptly indicates only that the calculation was not continued beyond that point; the periodic orbit family does continue. (a) Plots of the main symmetric families, also showing the beginnings of asymmetric branchings. The capital letters are the family names. The regions at the top of each of the A, H, I, and J families contains a small concentrated region of stability and instability. (b) Plot of the low-energy parts of the symmetric H, I, and J families of periodic orbits. (c) Plots of the simpler branchings from the V (vertical) and B (boomerang) families.

$$Q(E,\tau)=\int dE' \exp\left[-\frac{(E-E')^2}{2(\Delta E)^2}\right]\exp\left[\frac{i(E-E')\tau}{\hbar}\right]\rho(E')$$
$$=\sum_n \exp\left[-\frac{(E-E_n)^2}{2(\Delta E)^2}\right]\exp\left[\frac{i(E-E_n)\tau}{\hbar}\right]. \quad (2)$$

In the next sections we shall present alternative derivations of the quantal (E,τ) plot as well as its semiclassical interpretation. At present however, we shall simply use the expression Eq. (2). In Fig. 2(a), we show results for the Nelson potential (1) in an energy region where the classical dynamics is quite regular. The quantal calculation is shown as the contour lines of $|Q(E,t)|$, the classical version [which is the same as in Fig. 1(b)] is given by heavy lines for the stable periodic orbits, light lines for the unstable. It is clear that the ridges of the quantum calculation lie along the classical periodic orbits. Thus, with just the eigenvalues, we obtain the classical (E,τ) plot quite accurately. Details of this calculation as well as similar calculations at other values of E and τ will be given in Sec. V.

A. Wave packet derivation

The quantal plot as given by Eq. (2) was motivated by the semiclassical expression for the spectral density. Equivalently it may be motivated from the semiclassical dynamics of coherent states. This will allow for a rather intuitive understanding of the quantum plot in terms of the time evolution of particular coherent states.

We start with the Gaussian wave packet (or coherent state) $|\mathbf{p},\mathbf{q}\rangle$ at $t=0$. At time t it has evolved to

$$e^{-i\hat{H}t/\hbar}|\mathbf{p},\mathbf{q}\rangle \quad (3)$$

and the overlap of the evolved packet with the original one is

$$\langle\mathbf{p},\mathbf{q}|e^{-i\hat{H}t/\hbar}|\mathbf{p},\mathbf{q}\rangle. \quad (4)$$

This is large whenever the point $(\mathbf{p},\mathbf{q})$ is situated in phase space on or near a classical periodic orbit, of energy E_0, whose period τ_0 is close to t. (For example, see Figs. 12 and 15 of Ref. 16.) The overlap can be calculated semiclassically.[17] By expanding the phase in the semiclassical expression, it can be shown that the t-dependence for $t\approx\tau_0$ (i.e., locally in the region of the recurrence of the overlap) is proportional in lowest order to

$$e^{-iE_0(t-\tau_0)/\hbar}. \quad (5)$$

The Fourier transform in t will thus show a strong peak for energies close to E_0. However, we must again limit the integration, this time in t, to an interval where the approximation (5) holds. The Gabor transform of the overlap then becomes

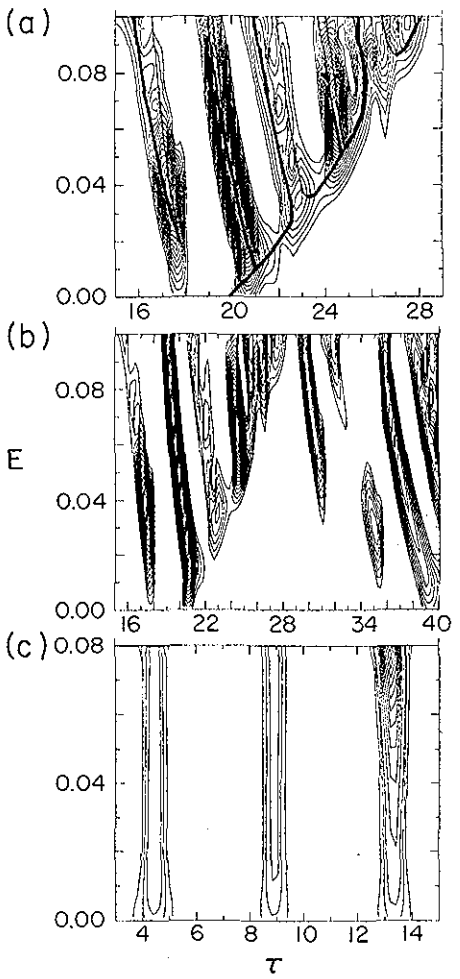

FIG. 2. Quantal and classical (E,τ) plots for the Nelson potential, with $\hbar=0.0025$ and $\Delta E=0.01$. This energy region is mostly regular. The figure shows the modulus of $Q(E,\tau)$ on a linear scale. (a) This plot shows the same (E,τ) region as in Fig. 1(b). All contours for the Nelson potential are in steps of 2 (unless otherwise noted), with 40 being the top contour. The quantal contours drawn here are 5–39. Heavy lines are stable orbits, light ones are unstable. (b) This is an extension of the time scale in (a). The quantal contours drawn are 7–39. (c) This plot shows the vertical orbit, which is a simple harmonic oscillator orbit along $x=0$ with period $\tau=4.443$. The quantal plot is also peaked at the second and third repetitions of this orbit, as well as at the period tripling which occurs at approximately $E=0.08$ [see Fig. 1(a)]. The quantal contours drawn are 1, 2, 3–25.

$$G(E,\tau;\mathbf{p},\mathbf{q})=\int dt\,\frac{1}{\Delta\tau\sqrt{2\pi}}\exp\left[-\frac{1}{2}\left(\frac{t-\tau}{\Delta\tau}\right)^2\right]\times\exp\left[\frac{iEt}{\hbar}\right]\langle\mathbf{p},\mathbf{q}|e^{-i\hat{H}t/\hbar}|\mathbf{p},\mathbf{q}\rangle. \tag{6}$$

This is a function of E and τ whose magnitude is large only when E is close to the energy, and τ is close to the period, of a periodic orbit selected by the wave packet $(\mathbf{p},\mathbf{q})$. In order to include all possible periodic orbits, we take the trace over the wave packets. Using

$$(2\pi\hbar)^{-2}\int\int d\mathbf{p}\,d\mathbf{q}\langle\mathbf{p},\mathbf{q}|e^{-i\hat{H}t/\hbar}|\mathbf{p},\mathbf{q}\rangle=\mathrm{Tr}[e^{-i\hat{H}t/\hbar}]=\sum_n e^{-iE_nt/\hbar} \tag{7}$$

the t integral becomes a simple Gaussian, and the resulting function is the same as Eq. (2) with

$$\Delta E=\frac{\hbar}{\Delta\tau}. \tag{8}$$

The two widths ΔE and $\Delta\tau$ are complementary and, obviously, they cannot both be small unless $\hbar$ is small.

B. Form factor derivation

As is evident from the discussion above, the quantal plot (2) has a resolution $\hbar$, as given by an area in the (E,τ) plane. As a result, the quantal plot will be a smeared approximation to the classical plot and only in the semiclassical limit of $\hbar\to 0$ the classical plot is recovered. We may, however, choose the two widths in energy and time independently, thus in principle allowing for a better resolution of the quantal plot even at fixed $\hbar$.

To this purpose, we start from the quantal form factor which is defined as the Fourier transform of the density–density correlation function (two-point cluster function[18]),

$$K(E,t)=2\pi\hbar\int d\epsilon e^{i\epsilon t/\hbar}\langle\rho_{\mathrm{osc}}(E+\epsilon/2)\rho_{\mathrm{osc}}(E-\epsilon/2)\rangle_\Lambda \tag{9}$$

and define a new quantal (E,τ) function as a smoothed form factor,

$$Q_2(E,\tau)=\int dt\,\frac{1}{\sqrt{2\pi}\lambda}\exp\left[-\frac{(\tau-t)^2}{2\lambda^2}\right]K(E,t)=2\pi\hbar\int d\epsilon\exp\left[\frac{i\epsilon\tau}{\hbar}-\frac{\epsilon^2\lambda^2}{2\hbar^2}\right]\times\langle\rho_{\mathrm{osc}}(E+\epsilon/2)\rho_{\mathrm{osc}}(E-\epsilon/2)\rangle_\Lambda. \tag{10}$$

In these expressions ρ_{osc} is the oscillating part of the spectral density, $\rho(E)=\langle\rho(E)\rangle+\rho_{\mathrm{osc}}(E)$, and Λ and λ are the energy and time widths, respectively. By working with correlations in $\rho_{\mathrm{osc}}(E)$ rather than $\rho(E)$, we avoid the singularity in the Fourier transform that otherwise arises (for $\lambda\to 0$) at $\tau=0$.

The spectral average in Eqs. (9) and (10) is with respect to the energy E. For simplicity we employ a Gaussian smoothing of width Λ,

$$\langle g(E)\rangle_\Lambda=\int dE'\,\frac{1}{\sqrt{2\pi}\Lambda}\exp\left[-\frac{(E-E')^2}{2\Lambda^2}\right]g(E'). \tag{11}$$

This procedure does not necessarily guarantee that $\langle\rho_{\mathrm{osc}}\rangle=0$. However, that will be true to the extent that we can neglect the energy dependence of the average density $\langle\rho(E)\rangle$.

With this simplification, the (smoothed) form factor then takes the form,

$$Q_2(E,\tau)=\frac{\sqrt{2\pi}\hbar}{\Lambda}\left\{\sum_{m,n}\exp\left[-\frac{1}{2\Lambda^2}\left(E-\frac{E_m+E_n}{2}\right)^2\right]\right.$$
$$\times\exp\left[-\frac{(E_n-E_m)^2\lambda^2}{2\hbar^2}\right]\exp\left[i\,\frac{(E_n-E_m)\tau}{\hbar}\right]$$
$$\left.-\frac{\hbar}{\lambda\Lambda}\exp\left[-\frac{\tau^2}{2\lambda^2}\right]\left[\sum_m\exp\left(-\frac{(E-E_m)^2}{2\Lambda^2}\right)\right]^2\right\}. \tag{12}$$

The last term in Eq. (12) arises from the average density of states. For λ small, it cancels the singularity at $\tau=0$ in the first term, and for $\tau\gg\lambda$, it is negligible. The two widths λ and Λ may be chosen at will. However, in order that the quantal (E,τ) plot reduces to the classical plot in the appropriate limit, $\hbar\to 0$, it is necessary that they both be small.

As it stands, Eq. (12) does not appear to be the same quantity that was derived in Eq. (2). However, in the special case that the two widths are "reciprocal,"

$$\Lambda=\frac{\hbar}{2\lambda}=\frac{\Delta E}{\sqrt{2}}, \tag{13}$$

$Q_2(E,\tau)$ in Eq. (12) is, apart from the contribution of the average density of states, equal to the absolute square of $Q(E,\tau)$ in Eq. (2). Note that this choice for the widths simplifies the numerical evaluation of the form factor, Eq. (12), as it reduces to a single sum over the eigenvalues E_n.

IV. SEMICLASSICAL LIMIT OF QUANTAL (E,τ) PLOT

In this section we will show that the quantum (E,τ) plots allow a simple semiclassical interpretation. In the expansion of Gutzwiller[1] the oscillating part of the spectral density is written as a sum over the primitive (i.e., nonrepeated) periodic orbits,

$$\rho_{\rm osc}(E)=\frac{1}{2\pi\hbar}\sum_p\tau_p(E)\sum_{\substack{n=-\infty\\ n\neq 0}}^{\infty}\frac{\exp[in(S_p(E)/\hbar-\mu_p\pi/2)]}{|\det(M_p^n(E)-1)|^{1/2}} \tag{14}$$

which as written applies to systems with only isolated periodic orbits. The quantities are the period (τ_p), monodromy or stability matrix (M_p), action (S_p) and Maslov index (μ_p) for each primitive periodic orbit (labeled by p) at energy E, and its repetitions, both positive and negative (labeled by n).

Neglecting problems of convergence we insert Eq. (14) in Eq. (10). It is now usually assumed[19] that in the semiclassical limit only the energy-dependence of the phases needs to be retained when the integral is carried out. This will not be correct near a bifurcation point where the amplitude is singular and the semiclassical approximation breaks down. In this case one needs to go beyond the simplest semiclassical approximation [Eq. (14)] and include higher order derivatives of the phase of the propagator (uniform approximation). This leads to the inclusion of "ghost" orbits in Eq. (14), which are complex continuations of the periodic orbits beyond the bifurcation where classical periodic orbits cease to exist.[20]

When we are not close to a bifurcation point, we may use the semiclassical approximation in Eq. (14). By taking the complex conjugate of $\rho_{\rm osc}(E+\epsilon/2)$ (which should be a real quantity), and expanding the actions:

$$S_j\left(E\pm\frac{\epsilon}{2}\right)\approx S_j(E)\pm\frac{\epsilon}{2}\frac{dS_j}{dE}=S_j(E)\pm\frac{\epsilon}{2}\,\tau_j(E) \tag{15}$$

we obtain the form

$$Q_2^{\rm sc}(E,\tau)=2\pi\hbar\int_{-\infty}^{\infty}d\epsilon\,\exp\left[i\,\frac{\epsilon\tau}{\hbar}-\frac{\epsilon^2\lambda^2}{2\hbar^2}\right]$$
$$\times\frac{1}{(2\pi\hbar)^2}\left\langle\sum_{j,k}\tau_j\tau_k A_j A_k^*\exp\left[i\left(\frac{S_j-S_k}{\hbar}\right.\right.\right.$$
$$\left.\left.\left.-(\mu_j-\mu_k)\,\frac{\pi}{2}\right)\right]\exp\left[-i\epsilon\,\frac{\tau_k+\tau_j}{2\hbar}\right]\right\rangle_\Lambda \tag{16}$$

where A_j is the amplitude factor from Eq. (14) that contains the monodromy matrix information. With this simplification, the integral is now easily performed and yields

$$Q_2^{\rm sc}(E,\tau)=\frac{1}{\sqrt{2\pi}\lambda}\left\langle\sum_{j,k}\exp\left[-\frac{1}{2\lambda^2}\left(\tau-\frac{\tau_k+\tau_j}{2}\right)^2\right]\right.$$
$$\left.\times\tau_j\tau_k A_j A_k^*\exp\left[i\left(\frac{S_j-S_k}{\hbar}-(\mu_j-\mu_k)\,\frac{\pi}{2}\right)\right]\right\rangle_\Lambda, \tag{17}$$

$$\approx\frac{1}{\sqrt{2\pi}\lambda}\left\langle\sum_k\tau_k^2|A_k|^2\exp\left[-\frac{(\tau-\tau_k)^2}{2\lambda^2}\right]\right\rangle_\Lambda. \tag{18}$$

In the last line we have assumed that as $\hbar\to 0$, the phases will give rapid oscillations that average to zero except for the diagonal terms. Equation (18) shows that the quantal plot is strongly peaked at values of E and τ that correspond to periodic orbits (or multiples thereof) $\tau\approx\tau_k(E)$, giving evidence that our intuitive expectations of the relation of the quantal plots [Eqs. (2) and (12)] to the classical (E,τ) plot are correct. In addition, we learn that the strength is determined by the stability exponent of the orbit, $|A_k|^2\approx\exp[-u_k]$, valid for large u_k. Hence the more unstable the orbit, the smaller the amplitude. Presumably, this diagonal approximation is only valid for $\tau\ll\hbar\langle\rho\rangle$ as we will discuss in the next section.

A. Validity of the diagonal approximation

The diagonal approximation is a result of the cancellation of phases in Eq. (17) when the semiclassical limit $\hbar\to 0$ is taken. The essential question is whether or not the phase difference in Eq. (17)

$$\frac{S_k-S_j}{\hbar} \tag{19}$$

can always be made large enough (as $\hbar\to 0$) so that energy averages of nondiagonal terms go to zero. The intuitive argument is that if $\hbar$ is fixed, there may be long periodic orbits with nearly equal periods (and consequently nearly equal

actions[21]) such that the phase difference is small and does not average away. If, on the other hand, the maximum period is fixed, then there is always a small enough $\hbar$ such that the diagonal approximation holds.

Berry investigated the regions of validity for the diagonal approximation by evaluating the spectral form factor. (His form factor differs slightly from ours.) In terms of the scaled time

$$\tilde{t} \equiv \frac{t}{\hbar \langle \rho \rangle} \tag{20}$$

he found that for

$$\tilde{t} \ll 1 \tag{21}$$

the diagonal approximation holds for both chaotic and integrable systems. On the other hand, by requiring that the trace formula should reproduce the average density of states he argued that for $\tilde{t} \gg 1$ the diagonal approximation should hold for integrable systems but fail for chaotic systems. For both regular and chaotic systems he found that $K(\tilde{t}) = 1$ for $\tilde{t} \gg 1$. However, the transition between these two time regimes is unknown. Taking the results from Random Matrix Theory as a guide, the transition between the two limits should depend on the time-reversal properties of the system, with time-reversal invariant systems (GOE) showing a smoother transition than systems without time-reversal invariance (GUE).[18]

V. NUMERICAL RESULTS

To check the validity of these approximations and verify the quantum–classical correspondence, we have calculated the quantal plot for three systems. Each system provides a unique testing ground: the Nelson Hamiltonian has a rich, well-known periodic orbit structure; the Hénon–Heiles Hamiltonian allows us to investigate the role of symmetries; and the Lipkin–Meshkov–Glick Hamiltonian provides a system where the quantum mechanics can more easily tell us about the classical mechanics than the other way around.

A. Nelson potential

As the first example of the quantal (E, τ) plot we choose the Nelson Hamiltonian, Eq. (1). The potential has a single well and the phase space is mostly regular for low energy, while for energies larger than $E \approx 0.3$ the phase space becomes predominantly chaotic. We present here the results for three different energy ranges. The quantum calculation was performed by diagonalizing in a basis of displaced harmonic oscillator states and its accuracy was checked by comparing the results with the Thomas–Fermi number of states.[22] The results are shown in Figs. 2–4 for the modulus of $Q(E, \tau)$, Eq. (2). In some cases periodic orbits are superimposed, with heavy lines for stable orbits and light lines for unstable orbits.

Figure 2 shows results for low energy, with most of the classical orbits in the regular region. The parameters used are $\Delta E = 0.01$ and $\hbar = 0.0025$, giving 1790 eigenstates below the energy $E = 0.1$. Figure 2(a) shows a range of E and τ for which the classical pattern is rather striking [see Fig. 1(b)]. The quantal pattern agrees perfectly with it. The maximum at

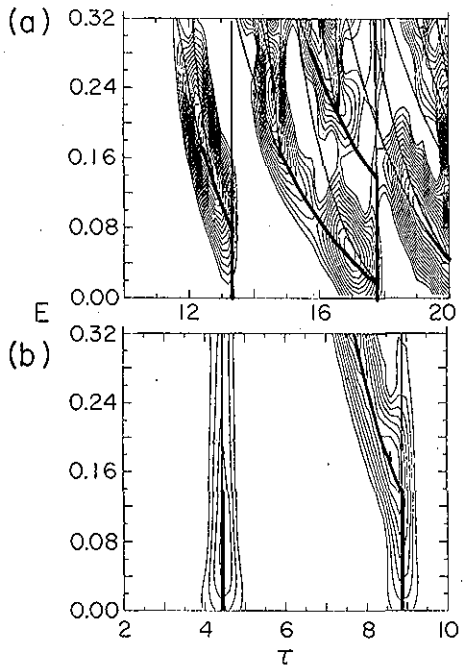

FIG. 3. Same as Fig. 2 with $\hbar = 0.01$ and $\Delta E = 0.04$. This energy region is classically mixed. (a) This plot shows a lower period, but higher energy regime than Fig. 2(a). The quantal contours drawn are 9–35. In (b), the vertical family is shown, with its second repetition, and its period doubling. The quantal contours are 2–10.

$E = 0.09, \tau = 26.3$ is not a disagreement; it corresponds to the twofold repetition of the periodic orbits present around $E = 0.09, \tau = 13$, associated with the period-tripling of the vertical orbit [see Figs. 1(a) and 2(c)]. Figure 2(b) shows a larger range of τ. Every feature for $\tau > 29$ can be recognized. In particular, the long ridge reaching the lower right corner is a twofold repetition of a similar ridge reaching the lower edge around $\tau = 20$. And the ridge at $\tau \approx 30$ is the period 7-tupling of the vertical orbit (not calculated in Ref. 10). Figure 2(c) shows the vertical orbit ($\tau = 4.443$), its twofold repetition, and its threefold repetition, with the period tripling showing up strongly at the top of the latter.

The second set of quantal plots is a medium-energy case, i.e., regularity and chaos are both present in appreciable amounts. The parameters are $\hbar = 0.01$ and $\Delta E = 0.04$. There are 1145 energy levels below $E = 0.32$. The results are given in Fig. 3. It is seen that all peaks of the quantal plot are located on a periodic orbit, usually in the vicinity of a bifurcation. Note that some classical orbits do not support a quantal ridge with the present resolution. These are the families of very unstable orbits. Figure 3(b) displays the quantal equivalent of the vertical orbit, and its period doubling at $E = 0.13$, yielding the "boomerang" periodic orbit. The period tripling and the period quadrupling appear prominently in Fig. 3(a).

In Fig. 4, we show the high-energy case, with phase space being almost entirely chaotic. The parameters are $\hbar = \sqrt{2}/17$, and $\Delta E = 0.2$, with 645 energy levels below $E = 2.0$. This time the quantal (E, τ) plot is not nearly as

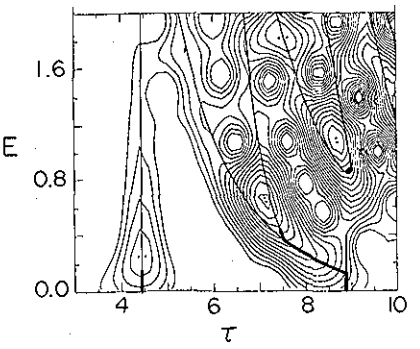

FIG. 4. *Same as* Fig. 2 *with* $\hbar=\sqrt{2}/17$ and $\Delta E=0.2$. This region is mostly chaotic. Extrema which are summits are marked with two dots, the other extremas are valleys. The quantal contours are 7–39.

distinct as in the other cases. It must be noted, however, in spite of the general messiness, that the classical lines correspond quite well to the ridges of the landscape, none of them traversing any of the many wells sprinkled around. Also, the two highest summits are situated very close to the two most important bifurcations.

For all of the calculations for the Nelson potential we would expect the diagonal approximation to hold, either because the classical dynamics is regular (Fig. 2), or in the chaotic regime because $\tilde{t}\ll 1$.

B. Hénon–Heiles system

Our second example is the well known Hénon–Heiles Hamiltonian[23]

$$H=\frac{p_x^2}{2}+\frac{p_y^2}{2}+\frac{x^2+y^2}{2}+x^2y-\frac{1}{3}y^3. \tag{22}$$

This potential has a bounded well for energies less than 1/6, and shows a steadily increasing chaotic fraction of phase space for energies above about 0.12. Many of the short periodic orbits were found by Huston *et al.*[24] The periodic orbits that will concern us here are the simple rotation, arcing libration, and straight libration. These are the only periodic orbits with energies below the dissociation energy and periods less than 9. The effect of these periodic orbits on the density of states was studied previously by Brack *et al.*[25]

The potential has a C_{3v} symmetry and accordingly the quantum states may be characterized by the irreducible representations to which they belong. The eigenvalues for $\hbar=0.0006$ were found by diagonalizing the Hamiltonian in a harmonic oscillator basis.

The quantal plot $Q_2(E,\tau)$, in Eq. (12), was calculated using all the eigenvalues and is shown in Fig. 5. The parameters used were $\Lambda=0.02$ and $\lambda=0.20$. The ridge located along $\tau=6.5$ corresponds to all three periodic orbits which begin at the same spot. The ridge at $\tau=13$ is the second repetition of these orbits. The peak near $\tau=0$ arises because the singularity there was not canceled completely.

As further evidence that we are truly seeing the periods of classical periodic orbits, we can look at the quantal plot for the different symmetry classes. With discrete symmetries

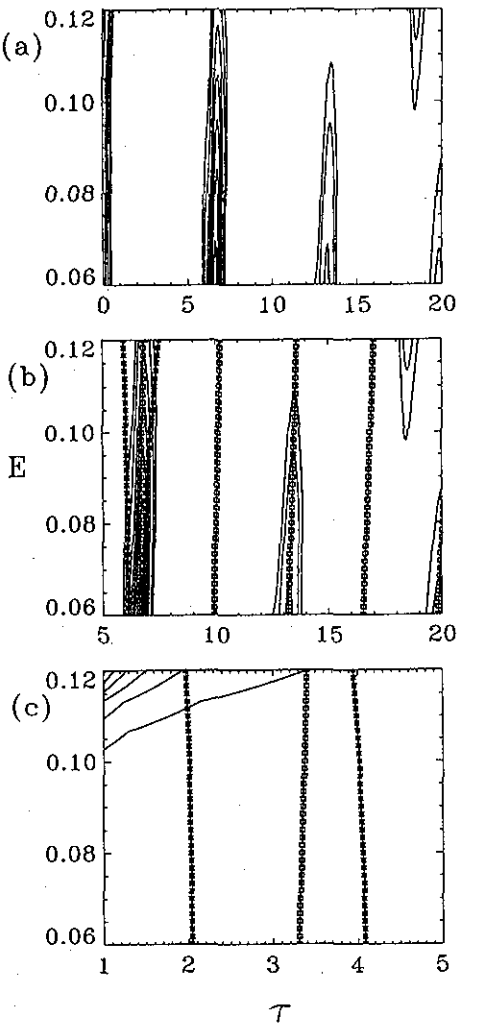

FIG. 5. The quantal and classical (E,τ) plot for the Hénon–Heiles Hamiltonian; the quantal calculation is shown by the contours of $Q_2(E,\tau)$ [Eq. (12)] using all eigenvalues. (a) This plot shows the entire region of interest. The three periodic orbits show up at $\tau=6.5$. (b) An enlargement of the region $5\leqslant\tau\leqslant 20$ is shown, along with the classical (E,τ) plot. The boxes indicate an unstable orbit, the stars a stable orbit. Only the orbits at $\tau=6.5$ are primitive, all others are repetitions of the unstable arcing libration. The classical plot was taken from the analytic formulas of Ref. 25. (c) An enlargment of the $1\leqslant\tau\leqslant 5$ region, with symmetry reduced orbits. Note that there appears to be no quantum analog to these symmetry reduced orbits.

present, the periodic orbit sum is modified.[26] The most important change that arises is that the periods that now appear in the semiclassical trace formula, Eq. (17) are the periods in the fundamental domain. From our derivation above, this means that we expect to see these shorter periods in the quantal plot. The period of the rotation periodic orbit is cut by a factor of 3, that of the arcing libration is cut in half, that of the straight libration remains the same. In Fig. 6 we show the quantal plots for the $A1$ symmetry class; in Fig. 7, the E symmetry class. (The $A2$ symmetry class carries essentially the same information as the $A1$ class, and is therefore not shown.) The rotation at $\tau\approx 2.1$ and its repetition at $\tau\approx 4.2$ show up in both plots; the arcing libration at $\tau\approx 3.2$ is missing from the E symmetry plot because the character of the

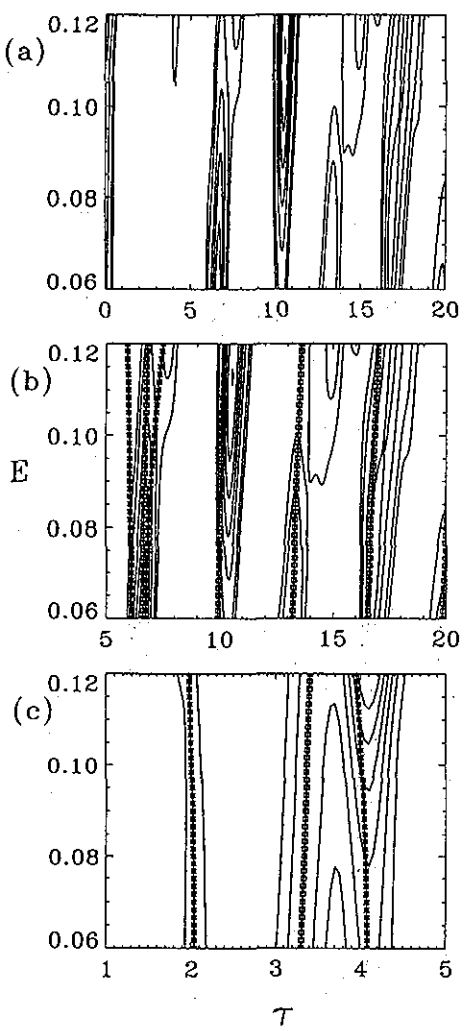

FIG. 6. Same as Fig. 5, except that the quantal calculations are done using only the eigenvalues with $A1$ symmetry. Note that for this symmetry class there is a quantum analog to the symmetry reduced orbits.

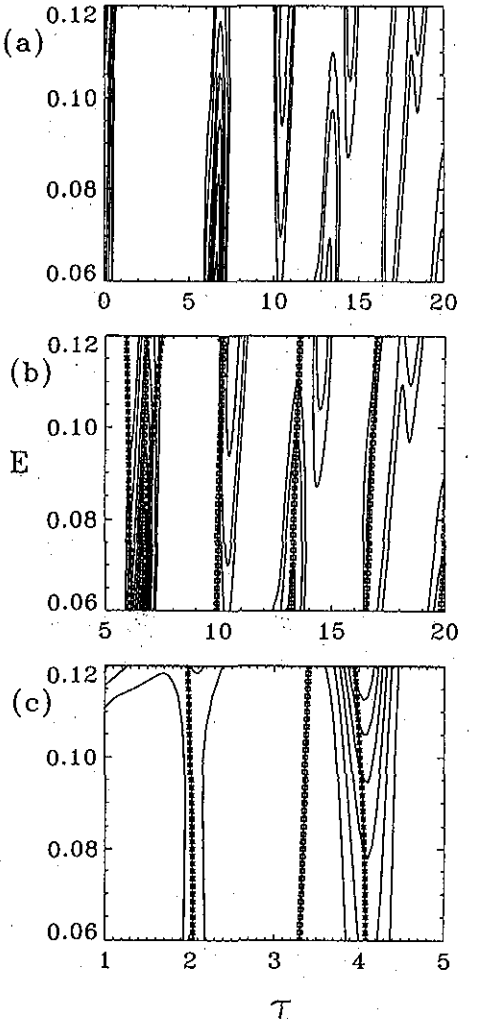

FIG. 7. Same as Fig. 5, except that the quantal calculations are done using only the eigenvalues with E symmetry. Note that for this symmetry class there is no quantum analog to the symmetry reduced arcing libration, but there is one for the rotation.

corresponding symmetry operation in the irreducible representation E is zero and the amplitude is proportional to the character.[26]

C. Lipkin–Meshkov–Glick model

This model is a quasispin model of a nucleus of N particles in three N-fold degenerate levels.[27] The quantum Hamiltonian is given by

$$\hat{H}=\sum_{k=0}^{2}\epsilon_k\left(\sum_{n=1}^{N}a_{kn}^{\dagger}a_{kn}\right)+\frac{V}{2}\sum_{k\neq l=0}^{2}\left(\sum_{n=1}^{N}a_{kn}^{\dagger}a_{ln}\right)^2 \tag{23}$$

where the first term is the single particle energy, and the second is the residual interaction. We examine the limit in which $\epsilon_i=0$ for $i=0,1,2$; in this case the classical Hamiltonian is

$$H(\mathbf{I},\boldsymbol{\theta})=I_1I_2\cos(\theta_2-\theta_1)+I_1(1-I_1-I_2)\cos(\theta_1)+I_2(1-I_1-I_2)\cos(\theta_2). \tag{24}$$

The variables I_i are the average number of particles in each level. This Hamiltonian is obtained by taking the expectation value of the quantum operator between coherent states in the limit of large N. The classical phase space is compact, corresponding to the finite number of quantum states. The classical limit is almost fully chaotic for $0\leqslant E\leqslant 0.2$, nearly integrable at both ends ($E\approx -1/4$ and $E\approx 1/3$), and mixed elsewhere. There has not been an exhaustive study of the periodic orbits of this system, however there are two periodic orbits which are found trivially.[28] These are the edge periodic orbits (with one $I_i=0$) and the symmetric periodic orbit (with $I_i=I_j$).

The quantum eigenvalues are obtained by straightforward diagonalization of the matrix in the Fock basis,[29] with $N=120$ (this is equivalent to $\hbar=0.1$). In the figures, only the 930 eigenvalues of the even–odd–odd symmetry class have been used; for details see Ref. 29.

Figure 8 shows the quantal plot which was made using Eq. (12) with $\Lambda=0.02$ and $\lambda=4$. The largest features of the quantal plot are as yet unknown. However, if we focus in on

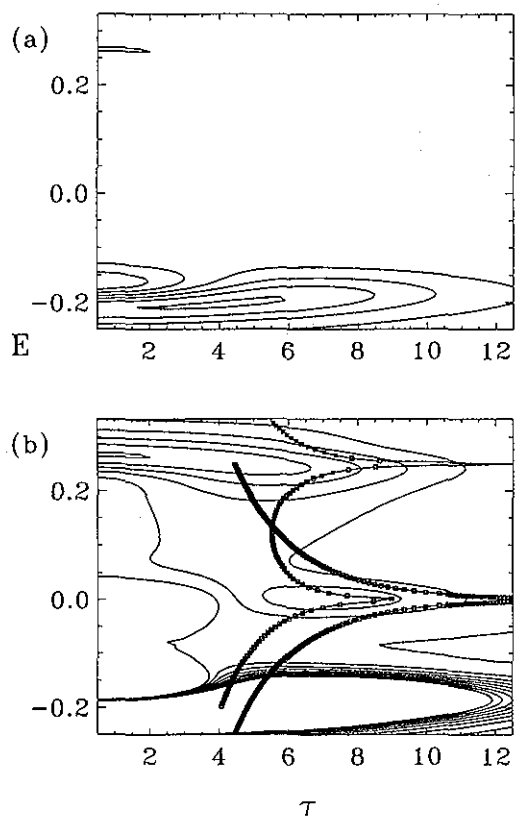

FIG. 8. (a) The quantal (E,τ) plot [Eq. (12)] for the Lipkin–Meshkov–Glick Hamiltonian using only the even–odd–odd states. (b) The same plot, but with the lower contours only. The lines indicate the known periodic orbits; stars indicate stable regions, squares indicate unstable.

the smaller features, we see [Fig. 8(b)] that there is a strong correspondence between the peaks in the quantal plot and the classical periodic orbits. As the orbit becomes very unstable (at large values of τ) the quantal amplitude dies off, as expected.

D. Discussion

From the numerical results above, we see that the correspondence between the classical and quantal plots is striking when the classical dynamics is regular (see Fig. 2 for the Nelson potential, and all plots for the Hénon–Heiles potential). As the degree of chaos is increased in the Nelson potential, the correspondence is less obvious. This can be understood from the semiclassical limit [Eq. (18)]. There we see that the amplitude depends inversely on the instability, so as the dynamics becomes globally more chaotic and the instability grows, the ridges along the periodic orbits begin to grow smaller and begin to fade into the background. Also, at a fixed energy we expect the most unstable orbits to show up the least in the quantal plots.

We also expect the quantum–classical correspondence to become more striking as $\hbar \to 0$ because the diagonal approximation is better in this limit. This is because the density of states scales as $(2\pi\hbar)^{-N}$ where N is the number of degrees of freedom; hence as $\hbar$ decreases, the condition for the diagonal approximation [Eq. (21)] is more likely to hold. Therefore, even when the classical dynamics is chaotic, the quantal plot will become sharper as the classical limit is approached.

These conclusions are also verified by the intuitions given by the wave packet discussion. Wave packets launched on periodic orbits will always recur (even for unstable orbits), but the recurrence is stronger the more stable the orbits or the smaller $\hbar$. Since the strong recurrence of wave packets is also the mechanism by which groups of wave functions are thought to be scarred,[30] periodic orbits which show up in the quantal (E,τ) plots should also scar groups of wave functions.

Peaks near the bifurcations, either isochronous or period-multiplying, can also be understood from Eq. (18). Isochronous bifurcations occur when the stability angle is a multiple of 2π. In a period n-tupling, the n-fold repeated orbit also has a stability angle of 2π. In either case, because the denominator is the sine of the stability angle, the amplitude becomes infinite. Of course this is not what occurs quantum mechanically, but a more complete semiclassical treatment[21] shows that the amplitude is indeed large at bifurcations.

VI. CONCLUSION

We have derived a quantal (E,τ) plot using three different approaches, and derived the semiclassical limit of this plot. In the diagonal approximation, it is clear that this plot must peak at the energy and period of classical periodic orbits. We have numerically verified the relation between the quantal plot and classical plot using three different model Hamiltonians and found that the agreement is striking in the regime where the classical dynamics is regular, and grows less distinct as the degree of chaos is increased. However, the relationship clearly holds in all regimes, and must improve as the classical limit is approached. Our method differs from similar work by others in that it uses only the energy levels and works for generic, nonscaling systems.

There are several open questions which we intend to pursue in future work. The first is an investigation of the quantal plots as we move into a regime where the diagonal approximation is not expected to hold. We also intend to study the periodic orbits in phase space or coordinate space in order to completely uncover the details of the periodic orbits; this will require, of course, the eigenvectors as well as the eigenvalues.

ACKNOWLEDGMENTS

This work was supported in part by funds provided by the U.S. Department of Energy under Contract No. DE-AC02-76ER03069. B.L. acknowledges support from the Institute for Nuclear Theory, University of Washington, where part of this work was performed. D.M. acknowledges the support of the Roland H. O'Neal Professorship. D.P. acknowledges support from the Center of Excellence in Molecular and Interfacial Dynamics (CEMAID).

[1] M. C. Gutzwiller, J. Math. Phys. **8**, 1979 (1967); **10**, 1004 (1969); **11**, 1791 (1970); **12**, 343 (1971).
[2] R. Balian and C. Bloch, Ann. Phys. **60**, 401 (1970); **64**, 271 (1971); **69**, 76 (1972).
[3] M. Tabor, *Chaos and Integrability in Nonlinear Dynamics* (Wiley, New

York, 1989); A. Ozorio de Almeida, *Hamiltonian Systems: Chaos and Quantization* (Cambridge University Press, Cambridge, 1988); M. C. Gutzwiller, *Chaos in Classical and Quantum Mechanics* (Springer-Verlag, New York, 1990); L. E. Reichl, *The Transition to Chaos: In Conservative Classical Systems: Quantum Manifestations* (Springer-Verlag, New York, 1992).

[4] M. V. Berry and J. P. Keating, J. Phys. A **23**, 4839 (1990); M. Sieber and F. Steiner, Phys. Rev. Lett. **67**, 1941 (1991).

[5] D. Wintgen, Phys. Rev. Lett. **58**, 1589 (1987).

[6] A. Holle, J. Main, G. Wiebusch, H. Rottke, and K. H. Welge, Phys. Rev. Lett. **61**, 161 (1988); M. L. Du and J. B. Delos, Phys. Rev. A **38**, 1896 (1988).

[7] N. Argaman, E. Doron, J. Keating, A. Kitaev, M. Sieber, and U. Smilansky, Phys. Rev. Lett. **71**, 4326 (1993).

[8] C. P. Malta, M. A. M. de Aguiar, and A. M. Ozorio de Almeida, Phys. Rev. A **47**, 1625 (1993).

[9] H. Poincaré, *Les Méthodes Nouvelles de la Mécanique Céleste* (Gauthier-Villars, Paris, 1892), Vol. I, Chap. III, Art. 36. Passage translated by M. Baranger.

[10] M. Baranger and K. T. R. Davies, Ann. Phys. **177**, 330 (1987).

[11] M. A. M. de Aguiar, C. P. Malta, M. Baranger, and K. T. R. Davies, Ann. Phys. **180**, 167 (1987).

[12] M. Baranger, K. T. R. Davies, and J. H. Mahoney, Ann. Phys. **186**, 95 (1988).

[13] D. Provost, Ph.D. thesis, Massachusetts Institute of Technology, September 1992.

[14] M. Saraceno (private communication, December 1992).

[15] Y. Meyer, *Wavelets: Algorithms and Applications* (SIAM, Philadelphia, 1993), pp. 63–64.

[16] S. Tomsovic and E. J. Heller, Phys. Rev. E **47**, 282 (1993).

[17] M. A. M. de Aguiar and M. Baranger, to be published.

[18] M. L. Mehta, *Random Matrices and the Statistical Theory of Energy Levels* (Academic, New York, 1972).

[19] M. V. Berry, Proc. R. Soc. London Ser. A **400**, 229 (1985).

[20] M. Kuś, F. Haake, and B. Eckhardt, Z. Phys. B **92**, 221 (1993); M. Kuś, F. Haake, and D. Delande, Phys. Rev. Lett. **71**, 2167 (1993).

[21] J. H. Hannay and A. M. Ozorio De Almeida, J. Phys A: Math. Gen. **17**, 3429 (1984).

[22] D. Provost and M. Baranger, Phys. Rev. Lett. **71**, 662 (1993).

[23] M. Hénon and C. Heiles, Astron. J. **69**, 73 (1964).

[24] T. E. Huston, K. T. R. Davies, and M. Baranger, Chaos **2**, 215 (1991).

[25] M. Brack, R. K. Bhaduri, J. Law, and M. V. N. Murthy, Phys. Rev. Lett. **70**, 568 (1993).

[26] B. Lauritzen, Phys. Rev. A **43**, 603 (1991); J. M. Robbins, Phys. Rev. A **40**, 2128 (1989).

[27] H. Lipkin, N. Meshkov, and A. J. Glick, Nucl. Phys. **62**, 188 (1965).

[28] P. Leboeuf and M. Saraceno, J. Phys. A: Math. Gen. **23**, 1745 (1990); P. Leboeuf and M. Saraceno, Phys. Rev. A **41**, 4614 (1990).

[29] D. C. Meredith, S. E. Koonin, and M. R. Zirnbauer, Phys. Rev. A **37**, 3499 (1988).

[30] E. J. Heller, Phys. Rev. Lett. **53**, 1515 (1984).